θ vacuum effects on chiral condensation and the η' meson correlators in two-flavor massive QED_2 on the lattice

Hidenori Fukaya and Tetsuya Onogi

Yukawa Institute for Theoretical Physics, Kyoto University, Kyoto 606-8502, Japan

(Received 4 April 2004; published 23 September 2004)

We study the scalar and pseudoscalar condensates and the η' meson correlators of the two-flavor massive Schwinger model in the $\theta \neq 0$ vacuum. Exploiting our new method which was developed to investigate topological effects in the previous work, we find that $\langle\bar{\psi}\gamma_5\psi\rangle^\theta \neq 0$ and there exists a long-range correlation of the η' meson. This phenomenon is well described by the clustering property. We also find that even in $\theta = 0$ case the cancellation of the long-range correlation is nontrivial and requires accurate contributions from higher topological sectors. Our results imply that the fluctuation of the disconnected diagram originates from the pseudoscalar condensate in each topological sector.

DOI: 10.1103/PhysRevD.70.054508 PACS numbers: 12.38.Gc, 11.15.Ha

I. INTRODUCTION

The topological structure is one of the essential aspects of the gauge theory. In addition to its theoretical importance, it has phenomenological implications in particle physics such as the η' meson mass and the θ vacuum in QCD. Although much is known in the instanton dilute gas approximation, in order to go beyond the level of qualitative understanding truly nonperturbative studies are required. For such purposes the lattice gauge theory should serve as a powerful tool, it has, however, been a nontrivial task to reproduce the topological structure since the naive lattice action does not preserve such properties.

Recently a new formulation of the lattice action has been proposed: the Ginsparg-Wilson fermion [1], which realizes the exact chiral symmetry and the chiral anomaly. Thus it would be an opportunity for the lattice gauge theory to provide a quantitative study of the topological structure of the gauge theories using this new formalism.

In this work we study the $n_f = 2$ massive Schwinger model using this new lattice formalism and the method developed in our previous work [2]. From the analytical studies of this model in the continuum space [3–9], it has been found that the pion mass and the chiral condensates at strong coupling and small θ behave as

$$\begin{aligned} m_\pi^\theta &= c_\pi m^{2/3} g^{1/3} \cos^{2/3}\frac{\theta}{2}, \\ -\langle\bar{\psi}\psi\rangle^\theta &= c_{\bar{\psi}\psi} m^{1/3} g^{2/3} \cos^{4/3}\frac{\theta}{2}, \\ i\langle\bar{\psi}\gamma_5\psi\rangle^\theta &= c_{\bar{\psi}\psi} m^{1/3} g^{2/3} \sin\frac{\theta}{2}\cos^{1/3}\frac{\theta}{2}, \end{aligned} \tag{1}$$

where g denotes a gauge coupling constant, m is the fermion mass, $\gamma_5 = \mathrm{diag}(1, -1)$, and c_π, $c_{\bar{\psi}\psi}$ are numerical constants. Although there have been extensive lattice studies on the massive Schwinger model, they are limited to the scalar condensate $\langle\bar{\psi}\psi\rangle$ and the η' meson masses in the $\theta = 0$ vacuum [10–19]. The lattice studies for the $\theta \neq 0$ vacuum done so far are only those in the pure U(1) gauge theory [20–26].

Our goal is to compute the scalar and the pseudoscalar condensates $\langle\bar{\psi}\psi\rangle$, $\langle\bar{\psi}\gamma_5\psi\rangle$, as well as the η' meson correlators $\langle\eta'^\dagger\eta'\rangle$ for fixed topological charges, and study how the practical lattice calculations reproduce physical quantities in the θ vacuum.

In Sec. II, we explain our method of simulations and how to evaluate the θ vacuum effects by reweighting. The results of the chiral condensate are presented in Sec. III. The connection between the η' correlators and the chiral condensates in each sector are shown in Sec. IV. In Sec. V, we also present our result of the η' meson correlators in the θ vacuum. The summary and the discussion are given in Sec. VI. The Appendix is devoted to the study of the topological susceptibility.

II. MONTE CARLO SIMULATIONS AND THE REWEIGHTING

In this section, we briefly explain our method of the simulation. More details can be found in our previous paper [2]. We take the gauge action proposed by Lüscher [27] and the domain-wall fermion action [28,29],

$$S = \beta S_G + S_F, \tag{2}$$

$$S_G = \begin{cases} \sum_P \frac{[1-\mathrm{Re}P_{\mu\nu}(x)]}{1-[1-\mathrm{Re}P_{\mu\nu}(x)]/\epsilon} & \text{if admissible} \\ \infty & \text{otherwise} \end{cases}, \tag{3}$$

$$\begin{aligned} S_F = \sum_{x,x'}\sum_{s,s'}\sum_{i=1}^{2}[&\bar{\psi}_s^i(x) D_{DW}(x, s; x', s')\psi_{s'}^i(x') \\ &+ \phi_s^{i*}(x) D_{AP}(x, s; x', s')\phi_{s'}^i(x')], \end{aligned} \tag{4}$$

where $\beta = 1/g^2$, $P_{\mu\nu}$ denotes the plaquette, ϕ's are Pauli-Villars regulators which cancel the bulk contribution of the domain-wall fermions, and ϵ is a fixed constant. The gauge fields generated by this action satisfy Lüscher's bound:

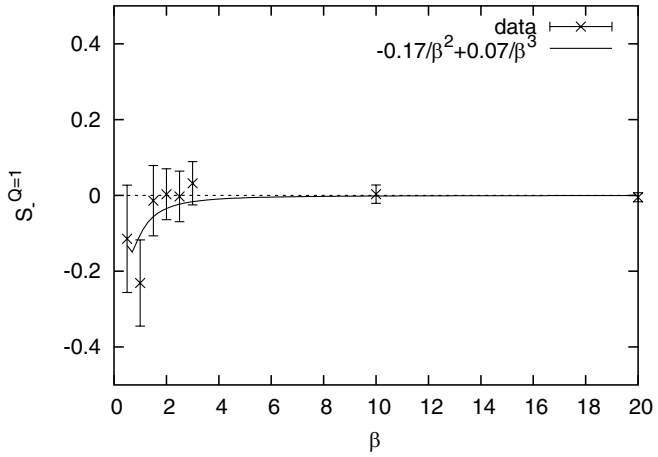

FIG. 1. Plot of $\Delta S^{Q=1}(\beta, m = 0.2)$. The solid line shows the result of the fit. ($a_1 = -0.17, a_2 = 0.07$, $\chi^2/\mathrm{dof} = 1.4$, $\int_{\beta=1.0}^{\infty} d\beta' \Delta S^1(\beta', m) = -0.14(11)$.)

$$1 - \mathrm{Re}P_{\mu\nu}(x) < \epsilon \quad \text{for all} \quad x, \mu, \nu. \tag{5}$$

Those gauge fields which satisfy the above condition are called "admissible." The "admissible" gauge fields have an exact topological charge defined as

$$Q \equiv \sum_x \frac{-i}{4\pi} \epsilon_{\mu\nu} \ln P_{\mu\nu}(x),$$

on the lattice if $\epsilon < 2$. This charge is never changed in the evolution in the hybrid Monte Carlo algorithm so that we can evaluate the observables in each sector separately. We take a $16 \times 16(\times 6)$ lattice at $\beta = 1.0$ and $\epsilon = 1.0$. Fermion mass is chosen as $m = 0.1, 0.15, 0.2, 0.25, 0.3$. Fifty molecular dynamics steps with a step size $\Delta\tau = 0.035$ are performed in one trajectory. Configurations are updated every ten trajectories. For each topological sector, around 500 trajectories are taken for the thermalization staring from the initial configuration which is the classical instanton solution with topological charge Q. We generate 300 configurations for each sector for the measurements and from 1000 to 10 000 for the reweighting factors at various β.

The expectation value of an operator O in the θ vacuum is expressed as

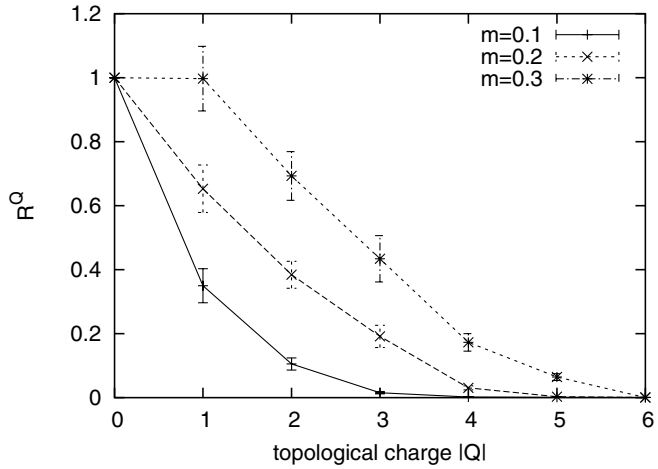

FIG. 2. The reweighting factors at $m = 0.1, 0.2, 0.3$ and $\beta = 1.0$.

$$\langle O \rangle^{\theta}_{\beta,m} = \frac{\sum_{Q=-\infty}^{+\infty} e^{iQ\theta} \langle O \rangle^{Q}_{\beta,m} R^Q(\beta, m)}{\sum_{Q=-\infty}^{+\infty} e^{iQ\theta} R^Q(\beta, m)}, \tag{6}$$

where $\langle\rangle^Q_{\beta,m}$ denotes the expectation value in the sector with Q at β, m and R^Q is the reweighting factor;

$$\begin{aligned} R^Q(\beta, m) &= \frac{Z_Q(\beta, m)}{Z_0(\beta, m)} \\ &= e^{-\beta S^Q_{G_{\min}}} \times \mathrm{Det}^Q \times e^{\int_\beta^\infty d\beta' \Delta S^Q(\beta', m)}, \end{aligned} \tag{7}$$

where Z_Q is the partition function in each sector,

$$\mathrm{Det}^{\,Q} \equiv \frac{\int dA^Q_{cl} \det(D + m)^2}{\int dA^0_{cl} \det(D + m)^2}$$

denotes the moduli integrals of the fermion determinants with topological charge Q, and $S^Q_{G_{\min}}$ is the action of the background. Det^Q's are calculated by the Householder method and the QL method [30]. The integrals of ΔS^Q which is defined as

$$\Delta S^Q(\beta', m) \equiv \langle S_G - S^Q_{G_{\min}} \rangle^Q_{\beta',m} - \langle S_G \rangle^0_{\beta',m}, \tag{8}$$

are evaluated by fitting the data with polynomials (See Fig. 1):

TABLE I. The reweighting factors $R^Q(\beta, m)$ at $\beta = 1.0$ for various topological sectors and the fermion masses.

	$m = 0.1$	$m = 0.15$	$m = 0.2$	$m = 0.25$	$m = 0.3$
R^0	1.000(0)	1.000(0)	1.000(0)	1.000(0)	1.000(0)
R^1	0.349(53)	0.74(12)	0.652(74)	0.78(14)	0.99(10)
R^2	0.105(19)	0.295(47)	0.384(42)	0.63(11)	0.693(76)
R^3	0.0154(34)	0.060(10)	0.191(34)	0.285(51)	0.434(72)
R^4	0.001 99(51)	0.0166(46)	0.0304(62)	0.129(25)	0.173(27)
R^5			0.003 17(63)	0.0346(70)	0.064(11)

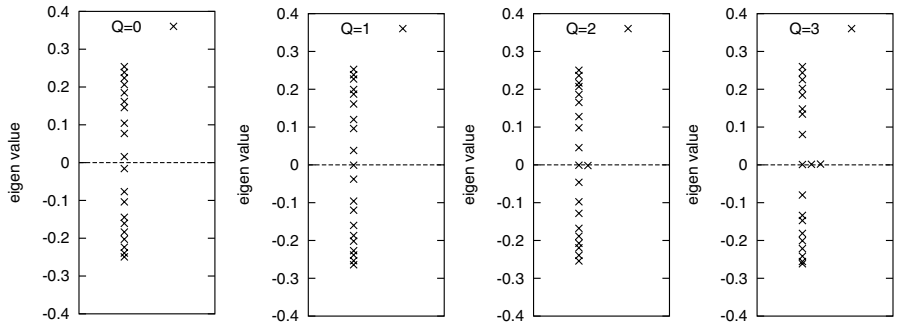

FIG. 3. The eigenvalues of the domain-wall Dirac operator $\gamma_5 D$ at $\beta = 1.0$ in each sector. The index theorem is realized very well.

TABLE II. The pion mass at $\beta = 1.0$ and $\theta = 0$.

	pion mass
$m = 0.1$	0.386(14)
$m = 0.15$	0.507(13)
$m = 0.2$	0.620(12)
$m = 0.25$	0.730(12)
$m = 0.3$	0.840(12)

$$\Delta S^Q(\beta', m) = \frac{a_1}{\beta'^2} + \frac{a_2}{\beta'^3}. \tag{9}$$

We present the Q dependence of R^Q in Fig. 2 and in Table I. The plots are consistent with the behavior indicated by the Atiyah-Singer index theorem. In Fig. 3 we show the lowest 20 eigenvalues with positive or negative chiralities of the massless domain-wall Dirac operator for a typical configuration in each topological sector. The smallest eigenvalues are consistent with exact zero at $O(10^{-3})$, which suggests that the index theorem is realized very well due to the smallness of the violation of chiral symmetries. As Fig. 2 indicates, we can ignore the contribution from large Q sectors. We evaluated the total expectation values by summing $-4 \le Q \le 4$ sectors for $m = 0.1, 0.15, 0.2$ and $-5 \le Q \le 5$ sectors for $m = 0.25, 0.3$.

III. THE CHIRAL CONDENSATES

We measure the chiral condensates $\langle\bar\psi\psi\rangle^Q_{\beta,m}$ and $\langle\bar\psi\gamma_5\psi\rangle^Q_{\beta,m}$ with the fixed topological charge. The total expectation values of them in the θ vacuum can be obtained by the following formula:

$$\begin{aligned}\langle\bar\psi\psi\rangle^\theta_{\beta,m} &= \frac{\sum_Q e^{iQ\theta}\langle\bar\psi\psi\rangle^Q_{\beta,m} R^Q(\beta, m)}{\sum_Q e^{iQ\theta} R^Q(\beta, m)}, \\ i\langle\bar\psi\gamma_5\psi\rangle^\theta_{\beta,m} &= \frac{\sum_Q e^{iQ\theta} i\langle\bar\psi\gamma_5\psi\rangle^Q_{\beta,m} R^Q(\beta, m)}{\sum_Q e^{iQ\theta} R^Q(\beta, m)}.\end{aligned} \tag{10}$$

In our practical calculation we truncate the sum over topological charge so that Q is restricted to be $|Q| \le Q_{\max}$ where $Q_{\max} = 4$ for $m = 0.1, 0.15, 0.2$, and $Q_{\max} = 5$ for $m = 0.25, 0.3$. The scalar and the pseudoscalar operators are defined as

$$\begin{aligned}\bar\psi\psi(x) &= \bar\psi(x, L_s)\psi(x, 0) + \bar\psi(x, 0)\psi(x, L_s), \\ \bar\psi\gamma_5\psi(x) &= \bar\psi(x, L_s)\psi(x, 0) - \bar\psi(x, 0)\psi(x, L_s),\end{aligned} \tag{11}$$

where $L_s = 6$ denotes the size of the extra dimension of the domain-wall fermions. In order to increase the statis-

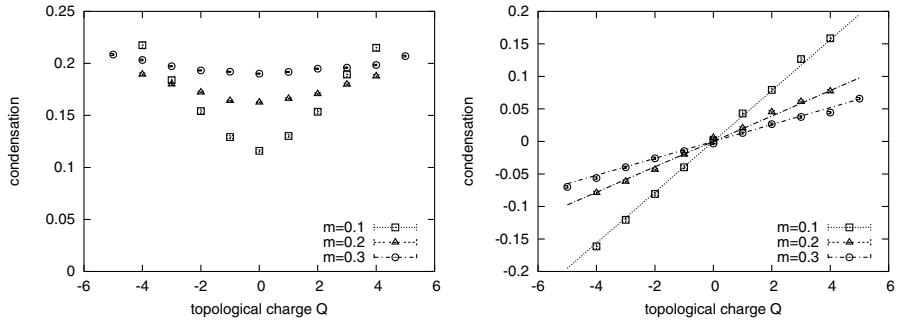

FIG. 4. Left: Lattice results of the condensate $-\langle\bar\psi\psi\rangle^Q$ at $\beta = 1.0$. It increases with $|Q|$ symmetrically. Right: Lattice results of the condensate $-\langle\bar\psi\gamma_5\psi\rangle^Q$ in each topological sector at $\beta = 1.0$. The lines show the prediction from the anomaly equation $-\langle\bar\psi\gamma_5\psi\rangle^Q = Q/(mV)$, which agrees with our data.

TABLE III. The scalar condensate $-\langle\bar{\psi}\psi\rangle^Q$ for a fixed topological charge Q at $\beta = 1.0$.

	$m = 0.1$	$m = 0.15$	$m = 0.2$	$m = 0.25$	$m = 0.3$
$-\langle\bar{\psi}\psi\rangle^0$	0.1160(13)	0.143 24(85)	0.162 51(68)	0.178 61(56)	0.190 18(48)
$-\langle\bar{\psi}\psi\rangle^1$	0.1302(14)	0.147 09(99)	0.166 19(78)	0.178 39(60)	0.191 81(52)
$-\langle\bar{\psi}\psi\rangle^{-1}$	0.1292(14)	0.148 52(95)	0.164 07(71)	0.179 92(65)	0.192 00(51)
$-\langle\bar{\psi}\psi\rangle^2$	0.1535(20)	0.1591(12)	0.170 68(97)	0.182 08(68)	0.194 90(58)
$-\langle\bar{\psi}\psi\rangle^{-2}$	0.1541(21)	0.1611(14)	0.172 23(84)	0.183 14(63)	0.193 26(55)
$-\langle\bar{\psi}\psi\rangle^3$	0.1894(26)	0.1758(15)	0.1798(12)	0.187 60(87)	0.195 92(62)
$-\langle\bar{\psi}\psi\rangle^{-3}$	0.1839(25)	0.1805(18)	0.1800(13)	0.190 51(89)	0.197 25(62)
$-\langle\bar{\psi}\psi\rangle^4$	0.2150(30)	0.1912(18)	0.1877(15)	0.195 26(98)	0.198 48(68)
$-\langle\bar{\psi}\psi\rangle^{-4}$	0.2175(29)	0.1933(18)	0.1895(13)	0.194 29(98)	0.203 34(78)
$-\langle\bar{\psi}\psi\rangle^5$				0.2040(12)	0.207 02(83)
$-\langle\bar{\psi}\psi\rangle^{-5}$				0.2030(11)	0.208 57(87)

TABLE IV. The pseudoscalar condensate $-\langle\bar{\psi}\gamma_5\psi\rangle^Q$ for a fixed topological charge Q at $\beta = 1.0$.

	$m = 0.1$	$m = 0.15$	$m = 0.2$	$m = 0.25$	$m = 0.3$
$-\langle\bar{\psi}\gamma_5\psi\rangle^0$	0.0014(20)	0.0001(19)	0.0058(18)	0.0045(19)	−0.0033(16)
$-\langle\bar{\psi}\gamma_5\psi\rangle^1$	0.0430(23)	0.0263(22)	0.0205(20)	0.0125(18)	0.0129(16)
$-\langle\bar{\psi}\gamma_5\psi\rangle^{-1}$	−0.0396(25)	−0.0288(20)	−0.0200(19)	−0.0181(18)	−0.0149(17)
$-\langle\bar{\psi}\gamma_5\psi\rangle^2$	0.0794(28)	0.0528(22)	0.0452(20)	0.0303(18)	0.0265(17)
$-\langle\bar{\psi}\gamma_5\psi\rangle^{-2}$	−0.0807(30)	−0.0584(23)	−0.0433(20)	−0.0349(17)	−0.0260(18)
$-\langle\bar{\psi}\gamma_5\psi\rangle^3$	0.1266(33)	0.0834(25)	0.0611(23)	0.0469(20)	0.0376(17)
$-\langle\bar{\psi}\gamma_5\psi\rangle^{-3}$	−0.1205(32)	−0.0896(26)	−0.0616(24)	−0.0524(20)	−0.0398(17)
$-\langle\bar{\psi}\gamma_5\psi\rangle^4$	0.1586(36)	0.1067(27)	0.0773(23)	0.0670(19)	0.0443(18)
$-\langle\bar{\psi}\gamma_5\psi\rangle^{-4}$	−0.1613(36)	−0.1094(28)	−0.0789(23)	−0.0637(20)	−0.0563(18)
$-\langle\bar{\psi}\gamma_5\psi\rangle^5$				0.0828(22)	0.0659(17)
$-\langle\bar{\psi}\gamma_5\psi\rangle^{-5}$				−0.0828(20)	−0.0700(18)

tics, spatial averages are always taken for the expectation values of local operators.

The condensates in each topological sector $\langle\bar{\psi}\psi\rangle^Q$ and $\langle\bar{\psi}\gamma_5\psi\rangle^Q$ are plotted in Fig. 4, where the numbers are given in Tables III and IV. It is obvious that the Q dependence of $\langle\bar{\psi}\psi\rangle^Q$ is symmetric and that of $\langle\bar{\psi}\gamma_5\psi\rangle^Q$ is antisymmetric, which can be understood from parity symmetry. The topological charge dependence of $\langle\bar{\psi}\gamma_5\psi\rangle^Q$ can be explained from the chiral anomaly equation given as

$$\partial_\mu A^\mu = 2mi\bar{\psi}\gamma_5\psi + \frac{i}{2\pi}\epsilon^{\mu\nu}F_{\mu\nu}. \tag{12}$$

Taking expectation values in the fixed topological sector and making summations over the whole spacetime volume, one obtains the following relation:

$$-\langle\bar{\psi}\gamma_5\psi\rangle^Q = Q/(mV), \tag{13}$$

which is in complete agreement with our lattice results. We also plot the ''reweighted'' condensates $\langle\bar{\psi}\psi\rangle^Q R^Q$ and $\langle\bar{\psi}\gamma_5\psi\rangle^Q R^Q$ in Fig. 5. It is important to note that most of the contributions in $i\langle\bar{\psi}\gamma_5\psi\rangle^{\theta\neq 0}$ come from $Q \neq 0$ sectors.

The fermion mass dependence of the total condensates $\langle\bar{\psi}\psi\rangle^{\theta=0}$ are presented in Fig. 6 in which we also plot the fit function:

$$f(m) = Am^B. \tag{14}$$

Figure 6 also shows the prediction from the analytic result of the continuum theory in Eq. (1) using m_π^2 as an input

$$-\langle\bar{\psi}\psi\rangle = \frac{c_{\bar{\psi}\psi}}{c_\pi^2 m}m_\pi^2. \tag{15}$$

In the following analysis we adopt the value of $c_{\bar{\psi}\psi}/c_\pi^2 = 1/(4\pi)$ by Hetrick *et al.*[7]. We find that our lattice results give a good agreement with the analytic results, as was also the case in the previous lattice studies [10–19].

We also present the θ dependences of the total condensates at $m = 0.15, 0.3$ as well as analytic results in Fig. 7 and Fig. 8. The numerical data are given in Tables V and VI. The qualitative features of the results in the continuum theory are realized in our simulation at small θ [See Eq. (1)]. Our lattice results show 30% deviation from the analytic results. Possible source of this discrep-

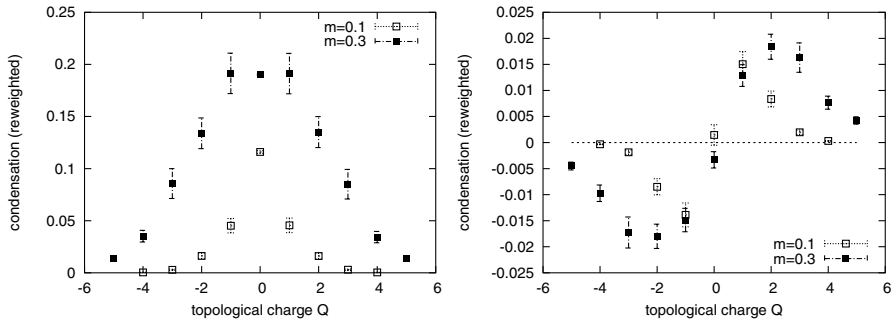

FIG. 5. Left: Reweighted condensate $-\langle\bar{\psi}\psi\rangle^Q R^Q$ in each topological sector at $\beta = 1.0$. Right: Reweighted condensate $-\langle\bar{\psi}\gamma_5\psi\rangle^Q R^Q$ in each topological sector at $\beta = 1.0$. Note that the largest contribution comes from $Q \neq 0$ sector.

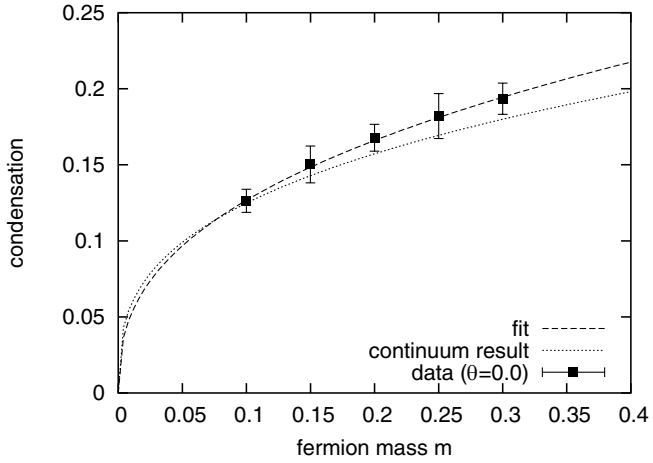

FIG. 6. The fermion mass dependence of $-\langle\bar{\psi}\psi\rangle^\theta$ at $\beta = 1.0$ and $\theta = 0$. The dashed line is the result of the fit with the function Am^B ($A = 0.311(36)$, $B = 0.388(68)$, $\chi^2/\mathrm{dof} = 0.068$.) The index B is consistent with $B = 1/3$ in the continuum theory. The dotted line is the prediction of the condensate from the relation $-\langle\bar{\psi}\psi\rangle^\theta = c_{\bar{\psi}\psi} m_\pi^2 / c_\pi^2 m$ with our data of m_π in Table II and $c_{\bar{\psi}\psi}/c_\pi^2 = 1/(4\pi)$ by Hetrick *et al.* [7].

ancy may be the discretization error or the error in the reweighting factor.

It should be mentioned that our method fails to give reliable data at large θ as seen in Fig. 7 and Fig. 8. As θ increases, the contributions from different topological sectors have different phases, which enhance the relative statistical errors. This problem would be more severe as the volume of the lattice increases. This so-called "sign problem" will have to be overcome when we try to go further to large θ and the large volume limit in the future works.

IV. THE η' MESON CORRELATORS AND THE CHIRAL CONDENSATES IN EACH TOPOLOGICAL SECTOR

The flavor singlet pseudoscalar meson η' is expected to be influenced by the topological properties of the vacuum. In QCD, the chiral anomaly gives a qualitative solution to the U(1) problem, and it has been a long standing issue whether the mass gap between the flavor singlet and nonsinglet pseudoscalars can really be explained quanti-

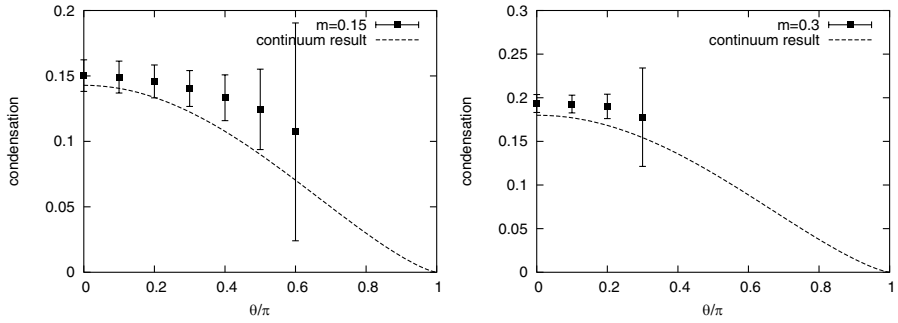

FIG. 7. The θ dependence of $-\langle\bar{\psi}\psi\rangle^\theta$ at $\beta = 1.0$ and $m = 0.15, 0.3$. The dashed line shows the continuum result $A\cos^{4/3}\frac{\theta}{2}$ where $A = 1/(4\pi)m_\pi^2$. Left: $m = 0.15$. Right: $m = 0.3$.

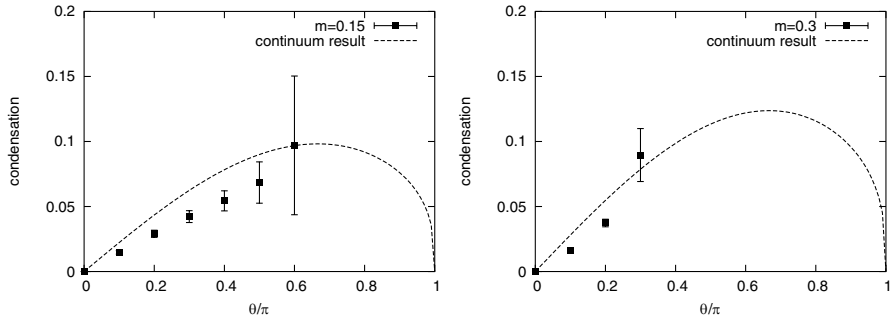

FIG. 8. The θ dependence of $i\langle\bar{\psi}\gamma_5\psi\rangle^\theta$ at $\beta = 1.0$ and $m = 0.15, 0.3$. The dashed line shows the continuum result $A\sin\frac{\theta}{2}\cos^{1/3}\frac{\theta}{2}$ where A is the same value of $-\langle\bar{\psi}\psi\rangle^\theta$. Left: $m = 0.15$. Right: $m = 0.3$.

TABLE V. The scalar condensate $-\langle\bar{\psi}\psi\rangle^\theta$ in θ vacuum at $\beta = 1.0$.

	$m = 0.1$	$m = 0.15$	$m = 0.2$	$m = 0.25$	$m = 0.3$
$-\langle\bar{\psi}\psi\rangle^{\theta=0}$	0.1338(93)	0.150(12)	0.1678(88)	0.182(15)	0.193(10)
$-\langle\bar{\psi}\psi\rangle^{\theta=0.1\pi}$	0.1309(90)	0.149(12)	0.1667(87)	0.181(15)	0.193(10)
$-\langle\bar{\psi}\psi\rangle^{\theta=0.2\pi}$	0.1219(87)	0.146(13)	0.1632(97)	0.177(19)	0.190(14)
$-\langle\bar{\psi}\psi\rangle^{\theta=0.3\pi}$	0.107(10)	0.140(14)	0.155(17)	0.166(47)	0.178(56)

tatively from the lattice calculation. For this reason a number of unquenched lattice QCD simulations with $n_f = 2$ to observe the mass gap [31–34] have been carried out.

The massive Schwinger model also has the mass gap between the flavor singlet and nonsinglet pseudoscalars due to the chiral anomaly. Since it is a two-dimensional theory, the numerical cost is much smaller than QCD and the disconnected diagrams can be evaluated explicitly without relying on the noise method [35] or the Kuramashi method [36]. The η' meson mass in $\theta = 0$ vacuum has been obtained using the overlap fermion [19].

The η' meson propagator is written as

$$\begin{aligned}\langle\eta'^\dagger(x)\eta'(y)\rangle &= \left\langle\left[-\sum_{f=1}^{2}\bar{\psi}_f\gamma_5\psi_f(x)\right]\left[\sum_{f=1}^{2}\bar{\psi}_f\gamma_5\psi_f(y)\right]\right\rangle \\ &= +2\left\langle\mathrm{tr}\left[\gamma_5\frac{1}{D}(x,y)\gamma_5\frac{1}{D}(y,x)\right]\right\rangle \\ &\quad - 4\left\langle\mathrm{tr}\left[\gamma_5\frac{1}{D}(x,x)\right]\mathrm{tr}\left[\gamma_5\frac{1}{D}(y,y)\right]\right\rangle,\end{aligned} \tag{16}$$

where the second term is the so-called disconnected part.

Figure 9 shows the propagators in each topological sector $\langle\eta'^\dagger(x)\eta'(0)\rangle^Q$. The result indicates the existence of long-range correlations. We evaluate them by fitting the data with the function

$$f(x) = A(e^{-Bx} + e^{-B(L-x)}) + C, \tag{17}$$

where $L = 16$ is the size of the lattice. We take $x \geq 3$ for the fitting range, we have also checked that the change of the value of C for different fitting range is small (less than 5%).

The data of C in each topological sector are listed in Table VII. The results for $m = 0.1, 0.2, 0.3$ are also plotted in Fig. 10. We find that there is a long-range correlation even in the $Q = 0$ sector. Moreover, it is remarkable that it gives the largest contribution to the total expectation value in the θ vacuum.

We would like to explain this phenomenon by clustering properties. Consider the two operators put on $t = T/2$ and $t = -T/2$ as Fig. 11. We expect that in the large volume limit the path integrals for the correlation func-

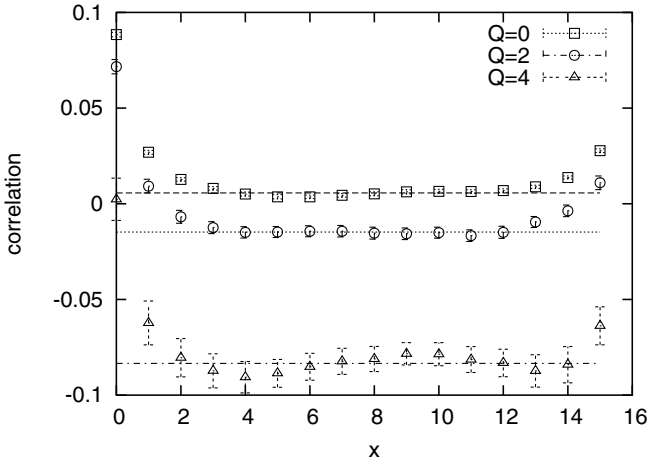

FIG. 9. The propagators of the η' meson in each topological sector at $\beta = 1.0$ and $m = 0.1$. Long-range correlations are seen. The lines are the results of the fit with the function in Eq. (17).

TABLE VI. The pseudoscalar condensate $i\langle\bar{\psi}\gamma_5\psi\rangle^\theta$ in θ vacuum at $\beta = 1.0$.

	$m = 0.1$	$m = 0.15$	$m = 0.2$	$m = 0.25$	$m = 0.3$
$i\langle\bar{\psi}\gamma_5\psi\rangle^{\theta=0}$	0.0(0)	0.0(0)	0.0(0)	0.0(0)	0.0(0)
$i\langle\bar{\psi}\gamma_5\psi\rangle^{\theta=0.1\pi}$	0.0122(10)	0.0147(28)	0.0166(12)	0.0180(16)	0.0159(11)
$i\langle\bar{\psi}\gamma_5\psi\rangle^{\theta=0.2\pi}$	0.0229(20)	0.0290(46)	0.0343(25)	0.0398(42)	0.0373(29)
$i\langle\bar{\psi}\gamma_5\psi\rangle^{\theta=0.3\pi}$	0.0306(28)	0.0422(77)	0.0521(49)	0.0739(16)	0.090(15)

TABLE VII. The long-range correlation $C^Q \equiv \lim_{|x|\to\text{large}}\langle\eta'^\dagger(x)\eta(0)\rangle^Q$ at $\beta = 1.0$ and $m = 0.1, 0.2, 0.3$. in each topological sector.

	$m = 0.1$	$m = 0.2$	$m = 0.3$
C^0	0.005 13(41)	0.002 71(50)	0.001 62(36)
C^1	0.000 10(56)	0.000 43(82)	0.001 19(43)
C^{-1}	0.0005(36)	0.000 30(48)	$-0.07e-3(63)$
C^2	−0.0151(12)	−0.003 97(97)	$-0.49e-3(54)$
C^{-2}	−0.0184(11)	−0.003 99(71)	$0.48e-3(44)$
C^3	−0.0489(33)	−0.0149(57)	−0.002 24(59)
C^{-3}	−0.0418(19)	−0.0110(18)	−0.006 58(68)
C^4	−0.0839(23)	−0.0242(10)	−0.0093(19)
C^{-4}	−0.0921(27)	−0.0271(18)	−0.0143(20)
C^5			−0.014 76(84)
C^{-5}			−0.020 55(79)

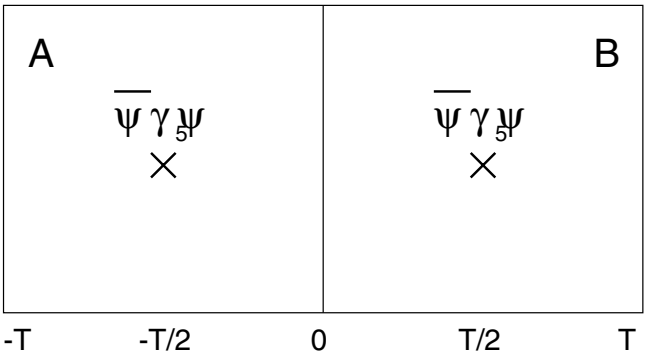

FIG. 11. The long-range correlation of the η' meson can be understood as a summation of the products of the condensates which are determined by the topological charge in the region A and B respectively: $Z_V^Q\langle\eta'^\dagger(T/2)\eta'(-T/2)\rangle^Q \to_{T\to\text{large}} - \sum_{Q'} Z_{V_2}^{Q'}\langle\bar{\psi}_f\gamma_5\psi_f\rangle_B^{Q'} Z_{V_1}^{Q-Q'}\langle\bar{\psi}_f\gamma_5\psi_f\rangle_A^{Q-Q'}$.

tions in the volume V can be expressed in terms of the chiral condensates as follows:

$$Z_V^Q\langle\eta'^\dagger(T/2)\eta'(-T/2)\rangle^{Q\overset{T\to\text{large}}{\longrightarrow}} - \sum_{Q'} Z_{V_2}^{Q'}\left\langle\sum_f\bar{\psi}_f\gamma_5\psi_f\right\rangle_B^{Q'} Z_{V_1}^{Q-Q'}\left\langle\sum_f\bar{\psi}_f\gamma_5\psi_f\right\rangle_A^{Q-Q'}, \tag{18}$$

where Z's denote the partition functions and $\langle\rangle_{A,B}^{Q'}$ means the expectation value in the region A, B with volume V_1, V_2 ($V = V_1 + V_2$). The gauge fields have a topological charge Q' in that region. In $Q = 0$ case taking $V_1 = V_2 = V/2$ we obtain

$$Z_V^0\langle\eta'^\dagger(T/2)\eta'(-T/2)\rangle^{Q=0\overset{T\to\text{large}}{\longrightarrow}} - \sum_{Q'} Z_{V/2}^{Q'}\left\langle\sum_f\bar{\psi}_f\gamma_5\psi_f\right\rangle_B^{Q'} Z_{V/2}^{-Q'}\left\langle\sum_f\bar{\psi}_f\gamma_5\psi_f\right\rangle_A^{-Q'} = +\sum_{Q'}(Z_{V/2}^{Q'})^2\left(\left\langle\sum_f\bar{\psi}_f\gamma_5\psi_f\right\rangle_A^{Q'}\right)^2 > 0, \tag{19}$$

where we assume $Z_{V/2}^Q = Z_{V/2}^{-Q}$, $\langle O\rangle_A^Q = \langle O\rangle_B^Q$ and we use the antisymmetry

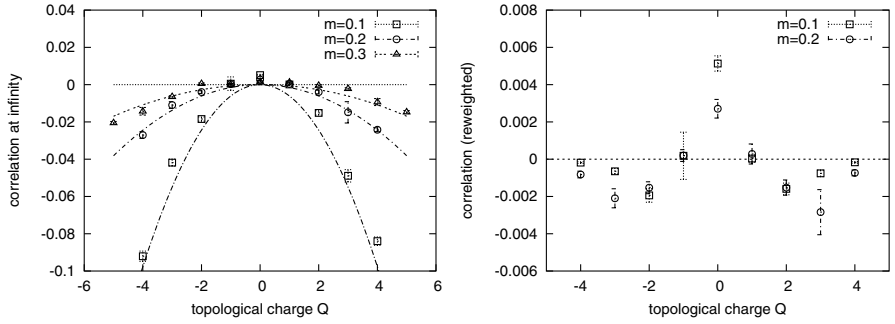

FIG. 10. Left: The long-range correlations in each topological sector. The lines show the Q dependence for large Q derived from the clustering property $\langle\eta'^\dagger(x)\eta'(0)\rangle^{Q\overset{|x|\to\text{large}}{\longrightarrow}} - 4Q^2/(mV)^2$, which agrees with our data quite well. Right: The long-range correlations (reweighted). It is interesting that the long-range correlation of $Q = 0$ sector is nonzero and gives the largest contribution to the total expectation value in the θ vacuum.

$$\langle\bar{\psi}\gamma_5\psi\rangle^Q = -\langle\bar{\psi}\gamma_5\psi\rangle^{-Q}, \tag{20}$$

as seen in Eq. (13) and Fig. 4. Moreover, the Q dependence of the long-range correlations for large Q and the large volume limit can also be understood. In this limit, since Q, V are extensive quantities, the free energy $F(Q, V)$ defined as $F = -\ln(Z_V^Q)$, which is another extensive quantity that should be expressed as

$$F = Vf\left(\frac{Q}{V}\right), \tag{21}$$

where f is some unknown function. Substituting Eq. (21) and approximating the sum over Q' by the integral over Q', we obtain

$$Z_V^Q\langle\eta'^\dagger(T/2)\eta'(-T/2)\rangle^{Q^{T\to\text{large}}} - \int dQ' \frac{2(Q-Q')}{mV_1} \times \frac{2Q'}{mV_2} e^{-[V_1 f(\frac{Q-Q'}{V_1})+V_2 f(\frac{Q'}{V_2})]}, \tag{22}$$

where we use Eq. (13) (see also Fig. 4). In the large volume limit, the integral over Q' is dominated by $Q'_* = \frac{QV_2}{V_1+V_2}$, which minimizes the total free energy. We can evaluate the integral by integrating the fluctuations of Q' around Q'_*. Changing variables as $Q' = Q'_* + q$ and expanding the free energy in q to the second order, the right hand side of Eq. (22) becomes

$$-\int dq \frac{4}{m^2}\left(\frac{Q^2}{V^2} - \frac{q^2}{V_1V_2}\right) e^{-[Vf(\frac{Q}{V})+\frac{Vq^2}{2V_1V_2}f''(\frac{Q}{V})]}, \tag{23}$$

where $V = V_1 + V_2$. Performing the integral over q to the first order we obtain

$$\langle\eta'^\dagger(T/2)\eta'(-T/2)\rangle^{Q^{T\to\text{large}}} - \frac{4}{m^2}\left[\frac{Q^2}{V^2} - \frac{1}{Vf''(\frac{Q}{V})}\right]. \tag{24}$$

The second term is indeed suppressed in the limit where both Q and the volume become large as expected. In Fig. 10, we compare our lattice results of the Q dependence of the long-range correlation and the first term in Eq. (24). It is surprising that this argument describes the results in Fig. 10 very well.

Thus we conclude that there is a relation between the long-range correlation of η' and the chiral condensates, which is understood by the clustering property of the theory based on the discussion of Q' instantons in the half of the space and $Q' - Q$ anti-instantons in the another half. Here we would like to emphasize two points:

(i) The η' meson has a long-range correlation in each topological sector even in $Q = 0$ case in spite of the fact that $\langle\bar{\psi}\gamma_5\psi\rangle^{Q=0}$ vanishes.

(ii) Our lattice data at large Q satisfy the following relation:

$$\langle\eta'^\dagger(x)\eta'(0)\rangle_V^{Q^{|x|\to\text{large}}} - \frac{4}{m^2}\frac{Q^2}{V^2}, \tag{25}$$

which can be explained by the clustering property.

As seen in Eq. (25), the long-range correlations in a specific topological sector are irrelevant in the infinite volume limit. Such "finite size" effects should, however, be treated with care in the numerical simulation where the lattice size is limited. Especially the volume dependence of observables due to topological effects is important, as Brower *et al.* indicate [37].

V. THE η' MESON IN THE θ VACUUM

From the discussion in Sec. IV, we expect that the correlation of the η' meson in the θ vacuum is expressed by the following function:

$$\langle\eta'^\dagger(x)\eta'(0)\rangle^\theta = A[e^{-m_{\eta'}x} + e^{-m_{\eta'}(L-x)}] + C_\theta. \tag{26}$$

We plot the data of $\langle\eta'^\dagger(x)\eta'(0)\rangle^\theta$ at $\theta = 0, 0.3\pi$, $m = 0.1$ in the left of Fig. 12. Fitting the data with Eq. (26), we evaluate the η' meson mass and the long-range correlation C_θ. The fitting range is determined as $x > 2$ from the effective mass at $\theta = 0$ (See Fig. 12).

As Fig. 13 and Table VIII show, the qualitative feature of the long-range correlations is consistent with $4|\langle\bar{\psi}\gamma_5\psi\rangle^\theta|^2$ at small m. Especially, it is remarkable that our data show the cancellation of the long-range correla-

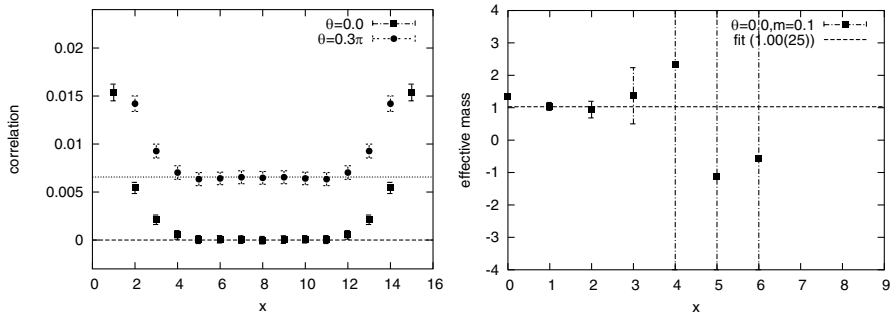

FIG. 12. Left: The propagations of the η' meson at $\theta = 0, 0.3\pi$ and $m = 0.1$ are shown. The lines show C_θ in Eq. (26). It is obvious that there are long-range correlations at $\theta \neq 0$. On the other hand, $\theta = 0$ case is consistent with zero. Right: The effective mass plot of the η' meson at $\theta = 0$ and $m = 0.1$. The dashed line shows the result of the fit in Eq. (26). The fitting range is $x \geq 2$.

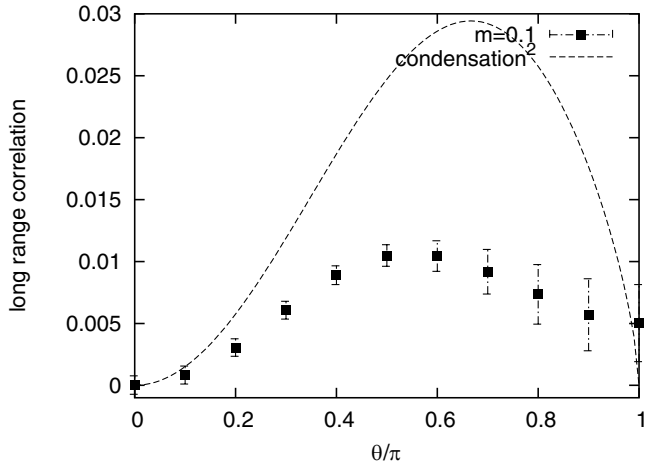

FIG. 13. The long-range correlations of the η' meson in the θ vacuum. The dashed line shows the result of $4|\langle\bar{\psi}\gamma_5\psi\rangle^\theta|^2$ in the continuum theory.

TABLE VIII. The long-range correlation $C^\theta \equiv \lim_{|x|\to\text{large}}\langle\eta^\dagger(x)\eta(0)\rangle^\theta$ at $\beta = 1.0$ and $m = 0.1, 0.15, 0.2$.

	$m = 0.1$	$m = 0.15$	$m = 0.2$
$C^{\theta=0}$	$0.03e-3(74)$	$-0.92e-3(46)$	$-0.001\,81(48)$
$C^{\theta=0.1\pi}$	$0.83e-3(72)$	$-0.91e-3(43)$	$-0.87e-3(38)$
$C^{\theta=0.2\pi}$	0.003 04(71)	0.002 38(47)	0.002 32(42)
$C^{\theta=0.3\pi}$	0.006 07(72)	0.006 30(75)	0.0089(16)
$C^{\theta=0.4\pi}$	0.008 89(75)	0.0112(15)	0.0180(45)
$C^{\theta=0.5\pi}$	0.010 48(88)	0.0171(35)	0.0143(49)

tions in the $\theta = 0$ vacuum at $m = 0.1, 0.15$. On the other hand, we find that it is difficult to evaluate them precisely as m increases since the Q dependence of the operator is steep ($\propto Q^2$). In fact, the long-range correlation at $m = 0.2$ gives 3.5σ deviation from zero. This is because one gets contributions from larger number of topological sectors as shown in Fig. 10 so that the cancellation becomes more delicate. Obviously the present level of accuracies for the reweighting factors R^Q and the condensate $\langle\bar{\psi}\gamma_5\psi\rangle$ are not sufficient for larger masses. Moreover, at $m = 0.25, 0.3$ the sectors with $|Q| > |Q_{\max}|$ cannot be ignored. In order to have a good control of the long-range correlation for larger masses, one has to reduce the statistical or systematic errors of R^Q and $\langle\bar{\psi}\gamma_5\psi\rangle$, while also evaluating higher topological sectors.

The data of the η' meson mass are presented in Fig. 14. They have large statistical errors but we find that the η' meson is indeed heavier than the pion as predicted by the continuum theory.

VI. SUMMARY AND DISCUSSION

We investigate the chiral condensates and the η' meson propagators in each topological sector and in the θ vacuum. Let us summarize the results as follows.

(1) The chiral condensates are nonzero in each sector,

$$-\langle\bar{\psi}\psi\rangle^Q \neq 0 \quad (Q \quad \text{symmetric})$$
$$-\langle\bar{\psi}\gamma_5\psi\rangle^Q = \frac{Q}{mV} \neq 0 \quad (Q \quad \text{anti-symmetric}), \tag{27}$$

where the second equation is consistent with the anomaly equation. The total expectation values in the θ vacuum obtained by the reweighting method are qualitatively consistent with the results of the continuum theory at small θ.

(2) There actually exist the long-range correlations of the η' meson in each sector,

$$\lim_{|x|\to\text{large}}\langle\eta'^\dagger(x)\eta'(0)\rangle^Q \neq 0, \tag{28}$$

even in $Q = 0$ case. It is also remarkable that our data show the following Q dependence of the long-range correlation as

$$\lim_{|x|\to\text{large}}\langle\eta'^\dagger(x)\eta'(0)\rangle^{Q=0} > 0,$$
$$\lim_{|x|\to\text{large}}\langle\eta'^\dagger(x)\eta'(0)\rangle^{Q>2} \sim -\frac{4Q^2}{m^2V^2} < 0, \tag{29}$$

which can be explained by the clustering property.

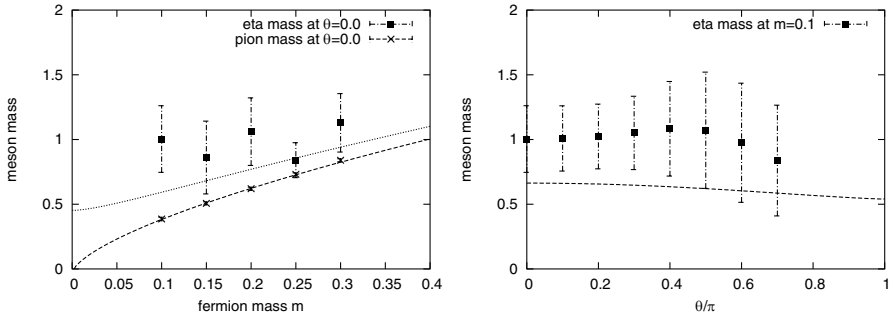

FIG. 14. Left: The η' meson mass and the pion mass at $\theta = 0$. The lines show the continuum results from Hosotani *et al.* [9] in which the effective coupling constant $g_{\text{eff}} = 0.68$ is determined from the pion mass at $m = 0.1$ and $\theta = 0$. Right: The θ dependence of the η' meson at $m = 0.1$.

This means that the precise measurements of higher topological sectors are necessary to cancel the long-range correlation in the total expectation value at $\theta = 0$ and finite V.

(3) Thus the η' meson correlations in the θ vacuum should be treated as the following function:

$$\langle \eta'^{\dagger}(x)\eta'(0)\rangle^{\theta} = A(e^{-m_{\eta'}x} + e^{-m_{\eta'}(L-x)}) + C_{\theta}, \tag{30}$$

even in the $\theta = 0$ vacuum. Our results of C_θ and $m_{\eta'}$ from the fit are qualitatively consistent with the continuum results as $\lim_{|x|\to\text{large}}\langle \eta'^{\dagger}(x)\eta'(0)\rangle^{\theta} \propto |\langle\bar{\psi}\gamma_5\psi\rangle^{\theta}|^2$, although there are discrepancies at the quantitative level.

It is now clear why the contribution from "disconnected" diagrams is very noisy. It is because each configuration gives the pseudoscalar condensate. They must be canceled at $\theta = 0$ by parity symmetry. We should, however, take the existence into account since our simulation would have both of the systematic and statistical errors in the evaluation of the higher topological sectors. Note that 4-dimensional QCD might have the same problems. It would be also important to investigate the topological effects on the $\bar{\psi}\gamma_5\psi$ condensate and the η' meson propagations in QCD.

It should be stressed that the present lattice formalism of the chiral fermion already allows us to study the topological effects as a well-defined problem in principle. Although our method may be limited to two dimensions, it would be important to investigate some new efficient method or algorithm for the study of the topological effect in QCD.

ACKNOWLEDGMENTS

The authors would like to thank H. Matsufuru, T. Umeda, Y. Kikukawa, S. Hashimoto, Y. Aoki , K. Takahashi and T. Takimi for useful discussions and comments. The authors also express special thanks to T. Izubuchi for crucial discussions on the relation between the chiral condensate and the anomaly equation. They would also like to acknowledge M. Hamanaka and S. Sugimoto for informing us of the analytic results on instantons and the massive Schwinger model. The authors thank the Yukawa Institute for Theoretical Physics at Kyoto University, where this work was initiated during the YITP-W-02-15 on "YITP School on Lattice Field Theory." The numerical simulations were done on NEC SX-5 at Research Center for Nuclear Physics in Osaka University, and Hitachi SR8000 model F1 supercomputer at KEK. This work was supported in part by a Grant-in-Aid for Scientific Research from the Ministry of Education, Culture, Sports, Science and Technology of Japan (No. 13135213). They would also like to thank the YITP members for constant encouragements.

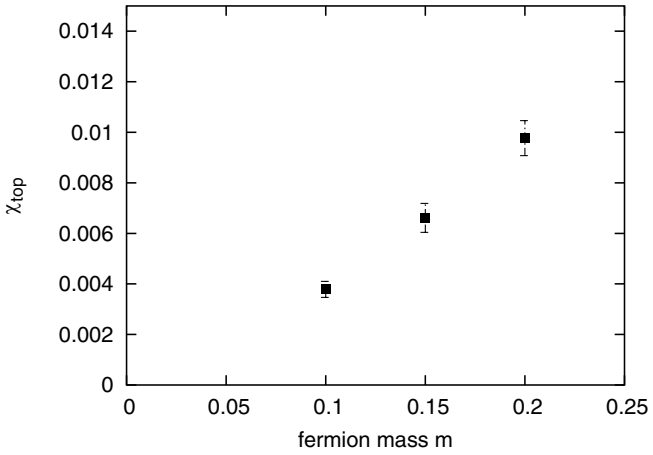

FIG. 15. The mass dependence of the topological susceptibility χ.

APPENDIX

In this appendix, we present our results of the topological susceptibility χ defined as

$$\chi \equiv \frac{1}{V}\langle Q^2\rangle. \tag{31}$$

The topological susceptibility is a useful measure of the topological fluctuations of the vacuum, which is extensively studied in QCD [38–46].

Figure 15 indeed shows a mass dependence of χ which decreases towards the chiral limit somewhat faster than linearly in m. It would be interesting to compare it with the analytical results. Recently, the topological susceptibility was also studied using the overlap fermion and staggered fermion [10], where they find χ decreases slower than linearly in m when the Leutwyler-Smilga parameter $x \equiv V\Sigma m$ is large.

[1] P. H. Ginsparg and K. G. Wilson, Phys. Rev. D **25**, 2649 (1982).
[2] H. Fukaya and T. Onogi, Phys. Rev. D **68**, 074503 (2003).
[3] J. S. Schwinger, Phys. Rev. **128**, 2425 (1962).
[4] S. R. Coleman, R. Jackiw, and L. Susskind, Ann. Phys. (N.Y.) **93**, 267 (1975).
[5] S. R. Coleman, Ann. Phys. (N.Y.) **101**, 239 (1976).

[6] A.V. Smilga, Phys. Rev. D **55**, 443 (1997).
[7] J. E. Hetrick, Y. Hosotani, and S. Iso, Phys. Lett. B **350**, 92 (1995).
[8] R. Rodriguez and Y. Hosotani, Phys. Lett. B **375**, 273 (1996).
[9] Y. Hosotani and R. Rodriguez, J. Phys. A **31**, 9925 (1998).
[10] S. Dürr and C. Hoelbling, Phys. Rev. D **69**, 034503, (2004).
[11] S. Dürr, Phys. Rev. D **62**, 054502 (2000).
[12] S. Elser, hep-lat/0103035.
[13] S. Elser and B. Bunk, Nucl. Phys. (Proc. Suppl.) **53**, 953 (1997).
[14] J. Kiskis and R. Narayanan, Phys. Rev. D **62**, 054501 (2000).
[15] S. Chandrasekharan, Phys. Rev. D **59**, 094502 (1999).
[16] C. Gattringer, Phys. Rev. D **53**, 5090 (1996).
[17] P. de Forcrand, J. E. Hetrick, T. Takaishi, and A. J. van der Sijs, Nucl. Phys. (Proc. Suppl.) **63**, 679 (1998).
[18] P. M. Vranas, Phys. Rev. D **57**, 1415 (1998).
[19] L. Giusti, C. Hoelbling, and C. Rebbi, Phys. Rev. D **64**, 054501 (2001).
[20] U. J. Wiese, Nucl. Phys. **B318**, 153 (1989).
[21] A. S. Hassan, M. Imachi, and H. Yoneyama, Prog. Theor. Phys. **93**, 161 (1995).
[22] A. S. Hassan, M. Imachi, N. Tsuzuki, and H. Yoneyama, Prog. Theor. Phys. **94**, 861 (1995).
[23] M. Imachi, T. Kakitsuka, N. Tsuzuki, and H. Yoneyama, hep-lat/9702018.
[24] J. C. Plefka and S. Samuel, Phys. Rev. D **56**, 44 (1997).
[25] V. Azcoiti, G. Di Carlo, A. Galante, and V. Laliena, Phys. Rev. Lett. **89**, 141601 (2002).
[26] M. D'Elia, Nucl. Phys. **B661**, 139 (2003).
[27] M. Lüscher, Nucl. Phys. **B549**, 295 (1999).
[28] D. B. Kaplan, Phys. Lett. B **288**, 342 (1992).
[29] Y. Shamir, Nucl. Phys. **B406**, 90 (1993).V. Furman and Y. Shamir, Nucl. Phys. **B439**, 54 (1995).
[30] S. A. Teukolsky, W.T. Vetterling, and B. P. Flannery, *Numerical Recipes in FORTRAN*, 2nd Ed., (Cambridge University Press, Cambridge, England, 1992).
[31] L. Venkataraman and G. Kilcup, hep-lat/9711006.
[32] UKQCD Collaboration, C. McNeile, and C. Michael, Phys. Lett. B **491**, 123 (2000); **551**, 391E (2003).
[33] TXL Collaboration, T. Struckmann, *et al.*, Phys. Rev. D **63**, 074503 (2001).
[34] CP-PACS Collaboration, V. I. Lesk *et al.*, Phys. Rev. D **67**, 074503 (2003).
[35] K. Bitar *et al.*, Nucl. Phys. **B313**, 348 (1989).H. R. Fiebig and R. M. Woloshyn, Phys. Rev. D **42**, 3520 (1990).
[36] Y. Kuramashi *et al.*, Phys. Rev. Lett. **72**, 3448 (1994).M. Fukugita *et al.*, Phys. Rev. D **51**, 3952 (1995).
[37] R. Brower, S. Chandrasekharan, J.W. Negele, and U. J. Wiese, Phys. Lett. B **560**, 64 (2003).
[38] H. Gausterer, J. Potvin, S. Sanielevici, and P. Woit, Phys. Lett. B **233**, 439 (1989).
[39] K. M. Bitar *et al.*, Phys. Rev. D **44**, 2090 (1991).
[40] Y. Kuramashi, M. Fukugita, H. Mino, M. Okawa, and A. Ukawa, Phys. Lett. B **313**, 425 (1993).
[41] UKQCD Collaboration, A. Hart, and M. Teper, Phys. Lett. B **523**, 280 (2001).
[42] TXL Collaboration, G. S. Bali *et al.*, Phys. Rev. D **64**, 054502 (2001).
[43] A. Hasenfratz, Phys. Rev. D **64**, 074503 (2001).
[44] B. Alles, M. D'Elia, and A. Di Giacomo, Phys. Lett. B **483**, 139 (2000).
[45] C. Bernard *et al.*, Phys. Rev. D **68**, 114501 (2003).
[46] UKQCD Collaboration, QCDSF Collaborations, and A. Hart, Phys. Rev. D **69**, 074510 (2004).